Dynamic Radio Map
Using Statistical Hypothesis Testing

Keita Katagiri , *Student Member, IEEE*, Koya Sato , *Member, IEEE*, Kei Inage, *Member, IEEE*, and Takeo Fujii , *Member, IEEE*

Abstract—Private fifth-generation mobile communication networks (5G) have garnered considerable attention for providing various communication services. In private 5G systems, such as those employed in smart factories, it is necessary to appropriately manage the interference power among diverse systems because each nonpublic operator deploys a gNodeB in the local area and utilizes a similar allocated frequency. Several researchers have discussed the use of a radio map, which stores the spatial distribution of received signal power values as a tool for managing intra-system interference. Radio maps are typically applied to television white space, where the location of the base station (BS) is fixed and the average value of the received signal power exhibits time-invariant characteristics. However, in private 5G networks, the estimation accuracy using a conventional radio map is lowered because the location of the BS may be changed when the factory is rearranged. In this study, a database server is used to infer a significant difference in the average values of the received signal power by means of Welch's *t*-test; the server then updates the radio map based on the test results. The simulation results indicate that the proposed method can detect changes in the BS location and update the radio map accurately.

Index Terms—Crowdsourcing, radio map, radio propagation, statistical hypothesis testing.

I. INTRODUCTION

RESEARCH and development toward fifth generation mobile communication networks (5G) are being actively conducted worldwide. 5G is the next-generation cellular system aimed at achieving high transmission speed, low latency, massive connectivity, and high reliability. Motivated by its unprecedented capability, several researchers have discussed a novel concept, referred to as *private 5G* (i.e., local 5G in Japan and industrial 5G in Europe), from the different viewpoints of industry, academia, and government [2], [3].
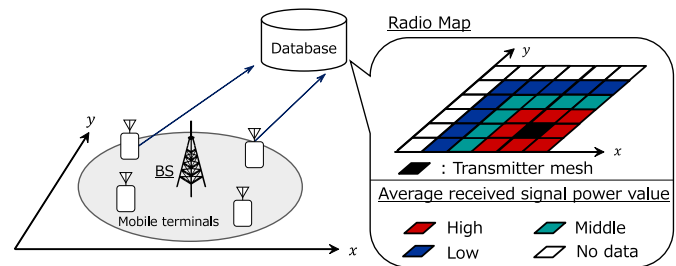
Fig. 1. A concept of the radio map.

In private 5G, multiple vendors will simultaneously deploy gNodeBs [4], which are 5G next-generation base stations (BSs), to support the new 5G radio communication. The communication services are provided through their gNodeBs over the same frequency band in a local area, such as a factory. Under these conditions, multiple transmitters would have to appropriately coordinate inter-transmitter interference to satisfy each demand. However, it is difficult to manage the interference accurately owing to the uncertainty in radio propagation caused by various factors, such as path loss and shadowing.

Recently, the concept of a *radio map* [5], [6] has attracted attention as an enabler for practical interference management. A radio map is defined as a map that visualizes the spatial distribution of the received signal power values. A crowdsourcing-assisted radio map has been the focus of research attention in recent years [7]–[12]. Fig. 1 illustrates the concept of this radio map. In this architecture, the database first collects the received signal power values from the spatially distributed mobile terminals. The database calculates the average of the received signal power values in the spatially distributed meshes to create a radio map.

A typical example of resource management based on a radio map includes a situation in which an interferer determines the transmission power such that its own interfering signal satisfies the criterion (i.e., the signal-to-interference power ratio) at the edge of the nearest other cell. Suppose the interferer knows only the path loss or shadowing variance. In this case, the interferer has to suppress its transmission power according to the path loss or shadowing variance. By contrast, if the radio map has precise information on both the path loss and shadowing values, the interferer does not need to suppress it. Although recently developed sophisticated techniques from the physical layer to the upper layers improve

the robustness of wireless systems against the ill effects of radio propagation, it has been reported that the spectrum sharing performance can be improved using an accurate radio map, even for 5G systems [13]–[15]. In this regard, several researchers revealed the achievable performance based on the channel state information [16]–[18]. Because the spectrum efficiency depends on the accuracy of the radio map, it is necessary to construct an accurate radio map for 5G systems, including private 5G systems.

Radio maps have mainly been applied to television white space [19]–[21], where the location of the BS is fixed and the average value of the received signal power exhibits time-invariant characteristics. Under this condition, the radio map that is initially constructed can accurately estimate the path loss and shadowing without updating the average values of the received signal power.

However, it is difficult to apply such an assumption in a private 5G scenario. Suppose that private 5G is employed in a factory and a construction site to monitor the production line and construction progress, respectively. In such situations, the manufacturing configurations, equipment, and construction environment may vary according to the product (e.g., vehicles and heavy machinery) and the construction progress from week to week or month to month [22]. This creates the need to rearrange the location of the private 5G system to monitor the reconstructed production line. Thus, the received signal power values may dynamically fluctuate owing to this rearrangement, and the initially constructed radio map would be rendered outdated. In the case of private 5G, multiple *uncoordinated* transmitters would be required to share a spectrum spatially while at the same time avoid inter-transmitter interference and guarantee their quality of service amidst changes in the transmitter positions. Because several situations may not allow each transmitter to estimate the change in the locations of other transmitters accurately, it is necessary to update the radio map after a period or event when using private 5G.

Similar studies have been conducted for other systems, such as wireless fidelity (Wi-Fi) and millimeter-wave communications. Methods to update the radio map for Wi-Fi positioning systems that utilize a radio map and the median access control address of each access point (AP) were proposed [23], [24]. However, the radio map cannot be updated when the location of a single BS is moved. This is because these methods update the radio map by detecting the installation of new APs or the removal of existing APs in an outdoor environment. A corresponding method for millimeter-wave systems was discussed [25]. This method determines the updating rate using the coherence duration. Consequently, the number of times the radio map is updated may significantly increase because the typical coherence duration is of the order of milliseconds. In addition, a real-time method to update a radio map was proposed [26]. Although this method can detect instantaneous changes in the surrounding environment by constantly positioning the mobile terminals and observing the radio environment, the observation cost, such as the time at which the observation of the radio environment occurred, increases significantly according to the range of the communication area.

Thus, although methods for updating the radio map have been proposed, they remain problematic in that they, for example, are unable to detect positional changes or have a high observation cost. In private 5G scenarios, such as in an industrial environment, the BS may continue to be repositioned after a few days or weeks to enable the production process to be monitored [27]. This makes it necessary to update the radio map; however, it is unnecessary to observe the radio environment in real time.

The application of machine learning (ML) techniques for radio map construction (e.g., [28]) has been discussed. However, many ML techniques, including long short-term memory, require prior preparation of a large dataset comprising labeled data for training; this implies that the transmission location and observation of the radio environment in cellular systems would repeatedly have to be changed. Thus, ML-based methods may not be suitable for cellular systems; in such systems, the main technical challenge is to accurately determine whether the radio map needs to be updated using *only real-time measurements*. Mo *et al.* [29] proposed a method based on kernel principal component analysis (KPCA) that can be used to update a radio map. This method extracts the features of the received signal power values based on the KPCA. However, when the number of measurement samples is less than the number of dimensions in KPCA, the inverse matrix cannot be calculated; that is, the environment in which we derive the eigenvalues may not be realistic.

Hypothesis testing [30], [31], which can be considered as a promising solution for solving the main technical challenges of applying ML-based methods for radio map construction, is classified into Bayesian hypothesis testing (BHT) [32]–[35] and statistical hypothesis testing (SHT) [36]–[39]. In BHT, it is necessary to model the prior distribution based on a priori information. However, in radio propagation, it is difficult to accurately model the prior distribution because the prior distribution of the average received signal power value depends on path loss, multipath fading, and shadowing.

SHT is classified further into parametric and non-parametric tests. Non-parametric testing cannot accurately infer the validity of the hypothesis if there is heteroscedasticity between the two populations [40]. In a practical wireless environment, it is unknown whether the variances of the received signal power samples are equivalent over the time domain. With regard to parametric testing, Lumley *et al.* [36] demonstrated the robustness of the *t*-test based on the central limit theorem. The *t*-test does not require the normality assumption for the population distribution, even if the number of samples used for inference is less than 100. However, the general *t*-test assumes homoscedasticity between the two populations.

In this article, motivated by the aforementioned difficulties, we propose a method for updating the radio map based on Welch's *t*-test [41], which is a hypothesis test. The proposed method uses Welch's *t*-test to enable the database server to infer a significant difference in the average received signal power values and updates the radio map based on the tested results. The main contributions of this article are summarized as follows.

1) We assessed conventional methods for updating the radio map, such as the BHT, a non-parametric method, and ML. Considering the need for real-time updating, the fact that the prior distribution does not have to be modeled, and that robustness for heteroscedasticity is required, we determined Welch's *t*-test to be appropriate for updating the radio map in cellular systems. The simulation results revealed that the proposed method can correctly infer the significant difference between two mean values, even with a small number of samples.

2) The validity of the radio map updating based on hypothesis testing was evaluated using the measured datasets. The emulation results reveal that the method based on hypothesis testing can accurately predict the radio environment compared with the methods based on unique averaging and forgetting factor.

The remainder of this article is organized as follows: Section II describes the system model and Section III explains the proposed method. In Section IV, we theoretically analyze the performance of the statistical power, and Section V describes the comparative methods. Section VI explains the simulation setups, and Section VII presents the simulation results. The emulation evaluation using the measured samples is discussed in Section VIII, and we conclude this article in Section IX.

II. SYSTEM MODEL

A. Conventional Radio Maps and the Associated Problems

In conventional radio maps, the values of the received signal power that are used for radio map construction are gathered in the cloud database deployed in the local or global area. The database server then divides the communication area into two-dimensional meshes and statistically processes the massive amounts of measurement data in each mesh. As the first step of radio map construction, the mobile terminals observe the properties of the radio environment such as the reception position and received signal power values in each location. The mobile terminals then report the observed datasets to the database server via their networks, such as Wi-Fi, to avoid communication congestion. Subsequently, the database server generates an initial radio map by utilizing the measurement datasets. Here, it is assumed that the surrounding environment, such as the location of the BS and positional relation of surrounding buildings, does not vary during the observation and after construction of the radio map. Thus, the initial radio map can accurately estimate the path loss and shadowing deviation without updating the average values of the received signal power.

However, in private 5G, such as that used in smart factories, the estimation accuracy based on the initial radio map decreases because the surrounding environment tends to vary after the radio map has been constructed.

B. Measurement Model

This study assumes that the database server updates the radio map using a simple algorithm and the minimum required external information. As in the case of private 5G, an outdoor smart factory is assumed. This system consists of a single BS and mobile terminals that are placed in the factory. The mobile terminals collect information such as the temperature and the values of the received signal power in each location and report the observed datasets to the database server. Subsequently, the database server constructs a radio map by averaging the reported datasets.[1]

Here, as the surrounding environment changes, we consider a situation wherein the location of the BS changes according to the manufacturing process. For readability, a *phase 0* and *phase 1* are defined as the environments before and after the BS is moved to a different location.

In this study, when the number of observed datasets becomes n_0 in the *m*th mesh, the database server calculates the average value of the received signal power in phase 0 for the *m*th mesh. After construction of the initial radio map, the mobile terminals repeatedly observe the radio environment in the same area and report the observed datasets to the database server. In the *m*th mesh, where the average received power is calculated in phase 0, the database server considers the newly reported datasets as time-series data $\boldsymbol{R}_m$ of the *m*th mesh. Subsequently, if the number of newly reported samples is more than n_1, $\boldsymbol{R}_m$ is divided such that the number of samples in each dataset is n_1 for hypothesis testing, which will be explained later. The time-series data $\boldsymbol{R}_m$ and divided dataset $\boldsymbol{R}_{m,T+k}$ are represented as

$$\boldsymbol{R}_m = \left(\boldsymbol{R}_{m,T}, \boldsymbol{R}_{m,T+1}, \cdots, \boldsymbol{R}_{m,T+N_s-1} \right), \quad (1)$$
$$\boldsymbol{R}_{m,T+k} = \left(P_{m,T+k,1}, \cdots, P_{m,T+k,n_1} \right),$$

where $T + k$ is the *k*th time $(k = 0, \cdots, N_s - 1)$ in the time series T, N_s is the number of time-series datasets, $P_{m,T+k,j}$ [dBm] is the *j*th instantaneous received signal power value of the *k*th time in the *m*th mesh.

In this study, we assume that the location of the BS changed over a period of a few weeks. Additionally, the observation period of the mobile terminals is a few days, and the observed datasets are reported to the database on the night after the observation. This is because the database server must update the radio map more frequently than the location changes of the BS.

III. PROPOSED METHOD

In this section, we present the proposed method. We first summarize hypothesis testing and Welch's *t*-test. Then, the radio map updating based on hypothesis testing is described.

A. Hypothesis Testing

In cellular systems, it may not be possible to obtain a large amount of training data in advance because it is difficult to repeat the changes in the transmission location and observations. Additionally, it may not be possible to model the prior distribution of the average received signal power accurately

---

[1]This study does not consider the effects of implementing a receiver. However, the measured values of the received signal power are affected by the individual differences between nodes [42]. This problem can be solved by introducing a calibration process. For more accurate radio map construction in a practical situation, the calibration technique is an optional choice.
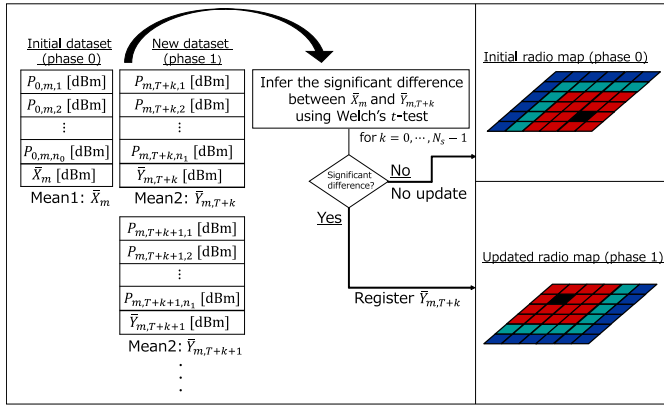
Fig. 2.   An overview of the proposed method.

owing to the uncertainty in the time-domain characteristics for radio propagation. Thus, it is essential to determine whether the radio map needs to be updated using only real-time measurements. As described in Section I, hypothesis testing can be considered as one of the tools for solving the task. In this study, we used Welch's *t*-test, which is an improved *t*-test, as it can accurately infer the significant difference between two mean values, regardless of the heteroscedasticity and homoscedasticity. In addition, Welch's *t*-test is recommended as being more suitable compared with the general *t*-test and non-parametric testing [43]. Fig. 2 presents an overview of the proposed method, in which the significant difference between the two mean values was inferred using Welch's *t*-test. The database server registers a new average value of the received signal power for the mesh only if a significant difference exists between the two mean values in the same mesh.

B. Welch's t-Test

Let Q_0 and Q_1 be the tested datasets with the sample mean values $\bar{X}_{\rm w}$ and $\bar{Y}_{\rm w}$, the unbiased sample variances $S_{0,\rm w}^2$ and $S_{1,\rm w}^2$, and the sample sizes n_0 and n_1, respectively. First, a null hypothesis H_0 and an alternative hypothesis H_1 are defined. In this study, we aimed to infer a significant difference between the two mean values. Thus, two hypotheses are defined as follows:

$$H_0 : \mu_{0,\rm w} = \mu_{1,\rm w}, \qquad (2)$$
$$H_1 : \mu_{0,\rm w} \neq \mu_{1,\rm w}, \qquad (3)$$

where $\mu_{0,\rm w}$ and $\mu_{1,\rm w}$ are the population means. Next, a *t*-value and a degree of freedom v are defined as

$$t = \frac{\bar{X}_{\rm w} - \bar{Y}_{\rm w}}{\sqrt{\frac{S_{0,\rm w}^2}{n_0} + \frac{S_{1,\rm w}^2}{n_1}}}, \qquad (4)$$

$$v \approx \frac{\left(\frac{S_{0,\rm w}^2}{n_0} + \frac{S_{1,\rm w}^2}{n_1}\right)^2}{\frac{\left(\frac{S_{0,\rm w}^2}{n_0}\right)^2}{n_0 - 1} + \frac{\left(\frac{S_{1,\rm w}^2}{n_1}\right)^2}{n_1 - 1}}. \qquad (5)$$

The *t*-value denotes the degree of similarity between the two distributions. If the difference between $\mu_{0,\rm w}$ and $\mu_{1,\rm w}$ is

significant, the *t*-value increases. The degree of freedom v corresponds to the variance of the Student's *t* distribution, as will be explained later. Under this condition, the probability distribution of the *t*-value is modeled as the Student's *t* distribution and its function is determined as follows:

$$f(t, v) = \frac{\Gamma\left(\frac{v+1}{2}\right)}{\sqrt{\pi v}\,\Gamma\left(\frac{v}{2}\right)} \left(1 + \frac{t^2}{v}\right)^{-\frac{v+1}{2}}, \qquad (6)$$

where $\Gamma(\cdot)$ is a gamma function. It should be noted that, because v is required to be an integer, it is rounded off if it is a decimal.

In Welch's *t*-test, a *p*-value is defined as the probability that a random variable $X \sim f(t,v)$ assumes a significantly higher or lower value than the calculated *t*-value as expressed by Eq. (4). Thus, the *p*-value corresponds to the tail of the Student's *t* distribution. In this study, the *p*-value is calculated in consideration of a two-sided test in which a rejection region exists in both tails of the Student's *t* distribution. In statistics, a one-sided test is generally used when the fluctuation of the population mean can be modeled deterministically. However, the fluctuation of the average received signal power value depends on the movement direction of the BS in phase 1. Thus, it is difficult to deterministically model the fluctuation of the average value of the received signal power in advance. In addition, in most cases, the two-sided test is statistically recommended as compared with the one-sided test. In the two-sided test, if the two-tailed *p*-value is less than the significance level α, the alternative hypothesis H_1 is accepted. The conditional inequality is represented as follows:

$$\int_{-\infty}^{-t} f(\xi, v)\, d\xi + \int_{+t}^{+\infty} f(\xi, v)\, d\xi < \alpha, \qquad (7)$$

where ξ is an integral variable, and the left side of the inequality describes the two-tailed *p*-value. If the difference between $\mu_{0,\rm w}$ and $\mu_{1,\rm w}$ is large, the *p*-value is close to zero, and the alternative hypothesis H_1 tends to be accepted.

C. Radio Map Updating Based on Welch's t-Test

In this study, $Q_{0,m}$ is defined as the instantaneous received signal power dataset of the *m*th mesh in phase 0, and its definition is given by

$$Q_{0,m} = \left(P_{0,m,1}, P_{0,m,2}, \cdots, P_{0,m,n_0}\right), \qquad (8)$$

where $P_{0,m,j}$ [dBm] is the *j*th instantaneous received signal power value of the *m*th mesh in phase 0.

Next, the dataset in phase 1 is explained. As described in Section II, the newly observed datasets are reported by mobile terminals on the night after the observation; substantial datasets may be obtained in each mesh. In Welch's *t*-test, the *p*-value decreased with an increase in the number of samples used for testing. Consequently, the alternative hypothesis H_1 tends to be accepted erroneously owing to the insignificant *p*-value. Thus, the database server performs hypothesis testing for each divided dataset $R_{m,T+k}$ expressed in Eq. (1) on the night after the observation. In this study, $Q_{1,m,T+k}$ is defined as $R_{m,T+k}$ of the *m*th mesh in phase 1. In addition,

$\bar{X}_m$ [dBm] and $\bar{Y}_{m,T+k}$ [dBm] are the average received signal power values of $\boldsymbol{Q}_{0,m}$ and $\boldsymbol{Q}_{1,m,T+k}$, respectively. Each average received signal power value can be expressed as:

$$\bar{X}_m = \frac{1}{n_0} \sum_{j=1}^{n_0} P_{0,m,j}, \tag{9}$$

$$\bar{Y}_{m,T+k} = \frac{1}{n_1} \sum_{j=1}^{n_1} P_{m,T+k,j}. \tag{10}$$

Here, each average received signal power value is calculated as the logarithmic value rather than the true value. This is because the alternative hypothesis H_1 cannot be accurately inferred owing to the existence of outliers. To calculate the t-value and the degree of freedom v, the unbiased sample variances $S_{0,m}^2$ and $S_{1,m,T+k}^2$ of $\boldsymbol{Q}_{0,m}$ and $\boldsymbol{Q}_{1,m,T+k}$ are defined as follows:

$$S_{0,m}^2 = \sum_{j=1}^{n_0} \frac{\left(P_{0,m,j} - \bar{X}_m\right)^2}{(n_0 - 1)}, \tag{11}$$

$$S_{1,m,T+k}^2 = \sum_{j=1}^{n_1} \frac{\left(P_{m,T+k,j} - \bar{Y}_{m,T+k}\right)^2}{(n_1 - 1)}. \tag{12}$$

Thereafter, the database server calculates the t-value and degree of freedom $v_{m,T+k}$ as follows:

$$t_{m,T+k} = \frac{\bar{X}_m - \bar{Y}_{m,T+k}}{\sqrt{\frac{S_{0,m}^2}{n_0} + \frac{S_{1,m,T+k}^2}{n_1}}}, \tag{13}$$

$$v_{m,T+k} \approx \frac{\left(\frac{S_{0,m}^2}{n_0} + \frac{S_{1,m,T+k}^2}{n_1}\right)^2}{\frac{\left(\frac{S_{0,m}^2}{n_0}\right)^2}{n_0 - 1} + \frac{\left(\frac{S_{1,m,T+k}^2}{n_1}\right)^2}{n_1 - 1}}, \tag{14}$$

where $t_{m,T+k}$ and $v_{m,T+k}$ are the t-value and degree of freedom of the mth mesh at the kth time, respectively. Under this condition, the calculated $t_{m,T+k}$ follows the Student's t distribution represented in Eq. (6) and the two-tailed p-value is calculated based on the left side of the inequality represented in Eq. (7).

The database server performs hypothesis testing using Eqs. (13), (14), and (7) in each mesh and determines whether the BS has been relocated during the night after the observation. If the alternative hypothesis H_1 is accepted in the mth mesh, the database server registers the new average received signal power value $\bar{Y}_{m,T+k}$ for the mth mesh. Here, the database server does not register $\bar{Y}_{m,T+k}$ when hypothesis H_1 is not accepted in the mth mesh. Consequently, the proposed method can accurately update the radio map with the minimum number of required updates.

It should be noted that if the number of datasets $\boldsymbol{R}_{m,T+N_s-1}$ is not n_1, hypothesis testing is not performed using $\boldsymbol{R}_{m,T+N_s-1}$. This is because the result of hypothesis testing strongly depends on the degree of freedom v, the value of which differs significantly depending on the number of samples n_1.

The proposed method computes Eqs. (9)–(12) to obtain the unbiased sample variances $S_{0,m}^2$ and $S_{1,m,T+k}^2$. Here, by substituting Eq. (9) into Eq. (11), we find that the computation of $S_{0,m}^2$ has a computational complexity of $\mathcal{O}(n_0^2)$, and that of $S_{1,m,T+k}^2$ is $\mathcal{O}(n_1^2)$. Therefore, the complexity of the proposed method is $\mathcal{O}(n_0^2 + n_1^2)$.

IV. STATISTICAL POWER ANALYSIS

In this section, we formulate the statistical power of the proposed method for quantitative evaluation. In Section IV-A, the probability distribution of the t-value and the statistical power is derived, after which the statistical power is evaluated using computer simulations.

A. Formulation of Statistical Power

The statistical power [30] is defined as the measure of the significant difference between two mean values ($\mu_{0,\text{w}}$ and $\mu_{1,\text{w}}$), and can be correctly inferred when the alternative hypothesis H_1, whether $\mu_{0,\text{w}} \neq \mu_{1,\text{w}}$, can be detected correctly. Thus, the statistical power indicates the cumulative distribution function (CDF) of the t-value. If the statistical power is high, the significant difference tends to be inferred correctly.

For the theoretical analysis, it was assumed that two datasets, $\boldsymbol{A}_0$ and $\boldsymbol{A}_1$, are obtained. We define each dataset as:

$$\boldsymbol{A}_0 = \left(P_{1,0}, P_{2,0}, \ldots, P_{n_0,0}\right), \ \boldsymbol{A}_1 = \left(P_{1,1}, P_{2,1}, \ldots, P_{n_1,1}\right), \tag{15}$$

where $P_{i,0}$ [dBm], and n_0 are the ith instantaneous received signal power and the number of samples in $\boldsymbol{A}_0$, respectively. Similarly, $P_{i,1}$ [dBm], and n_1 are the ith instantaneous received signal power and the number of samples in $\boldsymbol{A}_1$, respectively. Here, when the signals follow log-normal shadowing, $\boldsymbol{A}_0$ and $\boldsymbol{A}_1$ follow the log-normal distribution $LN(\mu_0, \sigma_0^2)$ and $LN(\mu_1, \sigma_1^2)$, respectively. Here, μ_0 [dBm] and μ_1 [dBm] are the logarithmic means, and σ_0 [dB] and σ_1 [dB] are the standard deviations, respectively.

First, when H_1 is correct, the t-value T_0 is given by

$$T_0 = \frac{\bar{X} - \bar{Y} - \delta}{\sqrt{\frac{S_0^2}{n_0} + \frac{S_1^2}{n_1}}}, \tag{16}$$

where $\bar{X}$ [dBm] and $\bar{Y}$ [dBm] are the sample means, and $\delta = \mu_0 - \mu_1$ [dB], S_0^2, and S_1^2 are the unbiased sample variances. Here, $\bar{X}$ and $\bar{Y}$ are defined as follows:

$$\bar{X} = \frac{1}{n_0} \sum_{i=1}^{n_0} P_{i,0}, \quad \bar{Y} = \frac{1}{n_1} \sum_{i=1}^{n_1} P_{i,1}. \tag{17}$$

Using the Welch–Satterthwaite equation [44], T_0 follows a non-central t distribution. In this study because a two-sided test was utilized, the CDF was calculated for both tails of the non-central t distribution. Thus, the statistical power $\pi(n_0, n_1, \delta)$

is represented as

$$\pi(n_0, n_1, \delta)$$

$$= 1 - \Pr\left(-t_{\hat{d}_{\mathrm{w}}}^{\frac{\alpha}{2}} \leq \frac{\frac{\bar{X}-\bar{Y}-\delta}{\sqrt{\frac{\sigma_0^2}{n_0}+\frac{\sigma_1^2}{n_1}}} + \frac{\delta}{\sqrt{\frac{\sigma_0^2}{n_0}+\frac{\sigma_1^2}{n_1}}}}{\sqrt{\frac{d_{\mathrm{w}}\frac{S_0^2}{n_0}+\frac{S_1^2}{n_1}}{\frac{\sigma_0^2}{n_0}+\frac{\sigma_1^2}{n_1}}}} \leq +t_{\hat{d}_{\mathrm{w}}}^{\frac{\alpha}{2}}\right)$$

$$\approx 1 - G_{\hat{d}_{\mathrm{w}},\lambda_{\mathrm{w}}}\left(+t_{\hat{d}_{\mathrm{w}}}^{\frac{\alpha}{2}}\right) + G_{\hat{d}_{\mathrm{w}},\lambda_{\mathrm{w}}}\left(-t_{\hat{d}_{\mathrm{w}}}^{\frac{\alpha}{2}}\right), \quad (18)$$

where d_{w} is a constant value, $G_{\hat{d}_{\mathrm{w}},\lambda_{\mathrm{w}}}(\cdot)$ is the CDF of the non-central t distribution with $\hat{d}_{\mathrm{w}}$ as the effective degree of freedom, λ_{w} the non-centrality parameter, and $t_{\hat{d}_{\mathrm{w}}}^{\frac{\alpha}{2}}$ the t-value calculated using $\hat{d}_{\mathrm{w}}$ (the proof for this result is detailed in the Appendix). Here, $G_{\hat{d}_{\mathrm{w}},\lambda_{\mathrm{w}}}(\cdot)$ is given by

$$G_{\hat{d}_{\mathrm{w}},\lambda_{\mathrm{w}}}(t') = \begin{cases} F_{\hat{d}_{\mathrm{w}},\lambda_{\mathrm{w}}}(t') & (t' \geq 0) \\ 1 - F_{\hat{d}_{\mathrm{w}},-\lambda_{\mathrm{w}}}(t') & (t' < 0), \end{cases} \quad (19)$$

where t' is a non-central t distributed random variable. $\hat{d}_{\mathrm{w}}$, λ_{w}, and $F_{\hat{d}_{\mathrm{w}},\lambda_{\mathrm{w}}}(t')$ are expressed by the following equations:

$$\hat{d}_{\mathrm{w}} \approx \frac{\left(\frac{S_0^2}{n_0}+\frac{S_1^2}{n_1}\right)^2}{\frac{\left(\frac{S_0^2}{n_0}\right)^2}{n_0-1}+\frac{\left(\frac{S_1^2}{n_1}\right)^2}{n_1-1}}, \quad \lambda_{\mathrm{w}} = \frac{\delta}{\sqrt{\frac{\sigma_0^2}{n_0}+\frac{\sigma_1^2}{n_1}}}, (20)$$

$$F_{\hat{d}_{\mathrm{w}},\lambda_{\mathrm{w}}}(t') = \Psi(-\lambda_{\mathrm{w}}) + \frac{1}{2}\sum_{j=0}^{\infty}\left[p_j I_y\left(j+\frac{1}{2}, \frac{\hat{d}_{\mathrm{w}}}{2}\right)\right.$$

$$\left. + q_j I_y\left(j+\frac{1}{2}, \frac{\hat{d}_{\mathrm{w}}}{2}\right)\right], \quad (21)$$

where $\Psi(\cdot)$ is the CDF of the standard normal distribution, and I_y is the regularized incomplete beta function. Here, p_j and q_j, respectively, are given by

$$p_j = \frac{1}{j!}\exp\left(-\frac{\lambda_{\mathrm{w}}^2}{2}\right)\left(\frac{\lambda_{\mathrm{w}}^2}{2}\right)^j, \quad (22)$$

$$q_j = \frac{\lambda_{\mathrm{w}}}{\sqrt{2}\,\Gamma\left(j+\frac{3}{2}\right)}\exp\left(-\frac{\lambda_{\mathrm{w}}^2}{2}\right)\left(\frac{\lambda_{\mathrm{w}}^2}{2}\right)^j. \quad (23)$$

It should be noted that the t distribution and the non-central t distribution are generally utilized in Welch's t-test if $\boldsymbol{A}_0$ and $\boldsymbol{A}_1$ follow a log-normal distribution. In the actual construction of the radio map, the shadowing component empirically follows a log-normal distribution. Thus, these distributions are relevant for the purpose of constructing the radio map.

B. Results

The theoretical statistical power was evaluated by conducting computer simulations. In this simulation, n_0 random samples were first obtained from $LN(\mu_0, \sigma_0^2)$. Next, n_1 random samples were obtained from $LN(\mu_1, \sigma_1^2)$. Then, Welch's t-test was performed considering a two-sided test; the number of times that $H_1 : \mu_0 \neq \mu_1$ is accepted was counted.
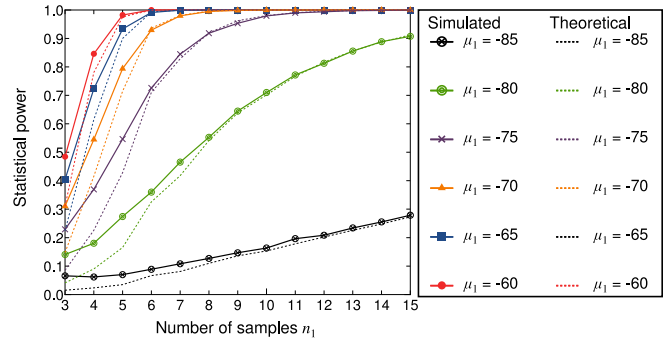

Fig. 3.   Theoretical and simulated statistical power.

We performed this trial 10,000 times and derived the simulated statistical power. The theoretical statistical power was calculated using Eq. (18).

Fig. 3 shows the theoretical and simulated results where $\mu_0 = -80.0$ [dBm], $\sigma_0 = \sigma_1 = 8$ [dB], $n_0 = 50$, and $\alpha = 0.01$. These results indicate that the difference between the theoretical and simulated values decreases according to the increase in n_1 (this difference is caused by the fluctuation of the sample mean). Moreover, the results show that a large difference between μ_0 and μ_1 makes it possible to correctly infer the significant difference with a small number of samples.

V. COMPARATIVE METHODS

This section describes the three comparative methods to assess the performance with respect to updating the radio map: the unique averaging-based method, forgetting factor-based method, and the Mann–Whitney U test (i.e., a non-parametric testing method).

A. Radio Map Updating Based on Unique Averaging

The unique averaging-based updating method [45], [46] is first considered. The database server calculates a new average received signal power value in each mesh using the following equation:

$$\bar{P}_{\mathrm{uni},m} = \frac{1}{n_{\mathrm{uni},m}}\left(\sum_{i=1}^{n_0} P_{0,m,i} + \sum_{k=0}^{N_s-1}\sum_{j=1}^{n_1} P_{m,T+k,j}\right), \quad (24)$$

where $\bar{P}_{\mathrm{uni},m}$ [dBm] is the updated value of the received signal power obtained by averaging the datasets in phase 0 and phase 1 of the mth mesh, and $n_{\mathrm{uni},m}$ is the number of received signal power samples stored for the mth mesh in phases 0 and 1. After periodic observation, the database server calculates the average received signal power value in each mesh using Eq. (24) without detecting the change in the BS location. Therefore, the number of radio map updates is very small. However, in smart factories, the difference between $P_{0,m,i}$ and $P_{m,T+k,j}$ may increase according to the distance the BS is moved in several meshes. Thus, the average received signal power value is updated inaccurately because of unique averaging.

B. Radio Map Updating Based on Forgetting Factor

The second comparative method for the radio map updating is the forgetting factor [47], [48]. The database server calculates a new average value for the received signal power in each mesh using the following equation:

$$
\begin{aligned}
\bar{P}_{\text{forget},m,T+k} = \eta\big(\bar{P}_{\text{forget},m,T+k-1}\big) \\
+ (1-\eta)\big(\mu_{1,m,T+k}\big),
\end{aligned} \tag{25}
$$

where $\bar{P}_{\text{forget},m,T+k}$ [dBm] is the updated average received signal power value at time $T+k$ of the mth mesh and $\bar{P}_{\text{forget},m,T+k-1}$ [dBm] is the updated average received signal power value at time $T+k-1$, and η is the forgetting factor. In this method, if a lower η is used, the newly observed average received signal power value is multiplied by a larger weight. However, the number of radio map updates is the highest because the forgetting factor-based method is required to sequentially update the average received signal power value N_s times in the mth mesh.

It should be noted that during the first update (i.e., $k = 0$), $\bar{P}_{\text{forget},m,T+k-1}$ is defined as $\tilde{X}_m$. In addition, the aforementioned calculation is not performed if the number of datasets $\boldsymbol{R}_{m,T+N_s-1}$ is not n_1. This is because the average received signal power value is inaccurately updated when the number of datasets $\boldsymbol{R}_{m,T+N_s-1}$ is significantly small.

C. Radio Map Updating Based on Mann–Whitney U Test

Finally, we will discuss the Mann–Whitney U test [49], a non-parametric testing method. In practice, the received signal power may not follow a typical probabilistic distribution (e.g., normal distribution) because of multipath fading, shadowing, and path loss. Because the Mann–Whitney U test can be utilized without assuming a typical distribution, this method was selected for comparative purposes. In addition, in the Mann–Whitney U test, a significant difference between the two datasets was inferred by sorting the measured samples. Welch's t-test infers a significant difference based on the difference between the two sample means, whereas the Mann–Whitney U test infers the difference based on the median values. In recent years, this test has been utilized in various fields [49]–[51].

However, the Mann–Whitney U test is reportedly inferior to Welch's t-test in terms of statistical power [52]. In other words, a significant difference may not be correctly inferred, even if the transmitter was to be moved by a large distance.

VI. SIMULATION SETUPS

Computer simulations were used to evaluate the accuracy of the proposed method. This section presents the radio propagation models and simulation procedures that were used.

A. Radio Propagation Models

The radio propagation models we used for phases 0 and 1 are defined as follows:

$$
\begin{aligned}
P_0(\boldsymbol{x}_{\text{Tx}}) = P_{\text{Tx}} - L_{0,\text{dB}}(d_0) - 10\gamma\log_{10}\left(\frac{d}{d_0}\right), \\
+ W_0 + F_0
\end{aligned} \tag{26}
$$

$$
\begin{aligned}
P_1(\boldsymbol{x}'_{\text{Tx}}) = P_{\text{Tx}} - L_{0,\text{dB}}(d_0) - 10\gamma\log_{10}\left(\frac{d'}{d_0}\right), \\
+ W_1 + F_1
\end{aligned} \tag{27}
$$

where $P_0(\boldsymbol{x}_{\text{Tx}})$ [dBm] and $P_1(\boldsymbol{x}'_{\text{Tx}})$ [dBm] are the instantaneous received signal power values in phase 0 and phase 1, respectively, P_{Tx} [dBm] is the transmission power of the BS, $d = \|\boldsymbol{x}_{\text{Tx}} - \boldsymbol{x}_{\text{Rx}}\|$ [m] is the link distance between the BS and a mobile terminal in phase 0, $d' = \|\boldsymbol{x}'_{\text{Tx}} - \boldsymbol{x}_{\text{Rx}}\|$ [m] is the link distance between the BS and a mobile terminal in phase 1, $\boldsymbol{x}_{\text{Tx}}$ and $\boldsymbol{x}'_{\text{Tx}}$ are the location of BS in phase 0 and phase 1, respectively, $\boldsymbol{x}_{\text{Rx}}$ is the location of the mobile terminal, d_0 [m] is the reference distance, γ is the path loss index, W_0 [dB] and W_1 [dB] are the log-normal shadowing in phase 0 and phase 1, respectively, and F_0 [dB] and F_1 [dB] are the small-scale fading in phase 0 and phase 1, respectively. Moreover, $L_{0,\text{dB}}$ [dB] is the free-space path loss, and its function is given by

$$
L_{0,\text{dB}}(d_0) = 10\log_{10}\left(\frac{4\pi d_0}{\lambda}\right)^2, \tag{28}
$$

where λ [m] is a wavelength.

Shadowing components are well known to have a spatial correlation in practice. If two terminals receive a signal from a fixed BS, the shadowing correlation $\rho_{i,j}$ is empirically formulated as an exponential decay model [53]. The shadowing correlation $\rho_{i,j}$ is generally modeled as follows:

$$
\rho_{i,j} = \exp\left(-\frac{\Delta d_{i,j}}{d_{\text{cor}}}\ln 2\right), \tag{29}
$$

where $\Delta d_{i,j}$ [m] is the distance between two terminals i and j, and d_{cor} [m] is the correlation distance, defined as a point on $\rho_{i,j} = 0.5$. A correlation distance of approximately 20 [m] was experimentally determined in an urban area [53]. Under spatial correlation shadowing, a probability distribution is modeled as a multivariate normal distribution [54] as follows:

$$
f_{\text{s}} = \frac{1}{\sqrt{(2\pi)^D \boldsymbol{\Sigma}}}\exp\left(-\frac{1}{2}(\vec{r}-\vec{p})^{\text{T}}\boldsymbol{\Sigma}^{-1}(\vec{r}-\vec{p})\right), \tag{30}
$$

where $\vec{r} = (r_0,\ldots,r_{D-1})^{\text{T}}$ is the average received signal power value vector, $\vec{p} = (p_0,\ldots,p_{D-1})^{\text{T}}$ is the median path loss vector, and D is the number of meshes. $\boldsymbol{\Sigma}$ denotes a $D \times D$ shadowing covariance matrix, as follows:

$$
\boldsymbol{\Sigma} = \begin{pmatrix} \sigma_{1,s}^2 & \cdots & \rho_{1,D}\sigma_{1,s}\sigma_{D,s} \\ \vdots & \ddots & \vdots \\ \rho_{D,1}\sigma_{D,s}\sigma_{1,s} & \cdots & \sigma_{D,s}^2 \end{pmatrix}, \tag{31}
$$

where $\sigma_{i,s}$ [dB] is the standard deviation of the shadowing from the BS to the ith terminal. In this simulation, each shadowing correlation of W_0 and W_1 is assumed to follow Eq. (29). Further, W_0 and W_1 are obtained by calculating the random values described in Eq. (30), respectively.

B. Simulation Procedures

The simulation procedures are summarized as follows:

a) The initial radio map in phase 0 is generated by averaging the instantaneous value of the received signal power represented in Eq. (26).

TABLE I
THE COMMON SIMULATION PARAMETERS

Communication area $E \times E$ [m²]	400×400
Mesh size [m²]	10×10
The number of meshes D	1600
The number of terminals M	20
The number of samples n_0	10
Transmission power P_{Tx} [dBm]	29
Path loss index γ	4.5
Reference distance d_0 [m]	10
Shadowing $\sigma_{i,s}$ [dB]	8
F_0 and F_1	i.i.d. Rayleigh fading
Center frequency [MHz]	3500
Noise floor [dBm]	-140
Forgetting factor η	0.1
Significance level α	0.01

b) *M* terminals are randomly placed in an $E \times E$ [m²] area and each terminal observes the value of the received signal power. Here, possible movement of the BS is determined randomly.

c) The database server uses Eqs. (13), (14), and (7) to infer whether the location of the BS in each mesh has changed.

d) The database server updates the average value of the received signal power for the mesh in which Eq. (7) is satisfied.

In the simulation, Step (a) was performed 1,000 times, and Step (b) to (d) were performed 1,000 times each time Step (a) was performed. Then, the accuracy of the updated radio map was evaluated. The common simulation parameters are listed in Table I.

Here, it is assumed that the positional relation of the surrounding buildings neither varies during the observation nor after construction of the radio map. This is because we aim to evaluate the accuracy of the updated radio map when the location of the BS changes.

It should be noted that the significance level α is set to 0.01, considering the typical α in hypothesis testing.

VII. SIMULATION RESULTS

In this section, we first present an example of an updated radio map. Subsequently, the estimation accuracy, the effect of the radio propagation characteristics, and Type I and II errors are described.

A. *Example of Radio Map Construction*

Examples of radio maps are presented in Fig. 4; Figs. 4(a) and 4(b) were constructed by averaging 10,000 received signal power samples for each mesh in phase 0 and phase 1, respectively. Here, n_1 and d_{cor} are 50 and 20 [m], respectively, and the BS was repositioned 300 [m] to the left. Figs. 4(b), 4(d), and 4(f) reveal that the average received signal power can be accurately updated in both Welch's *t*-test and the Mann–Whitney *U* test. However, in Fig. 4(f),

(a) True map (phase 0).   (b) True map (phase 1).

(c) Welch (phase 0).   (d) Welch (phase 1).

(e) Mann–Whitney (phase 0).   (f) Mann–Whitney (phase 1).

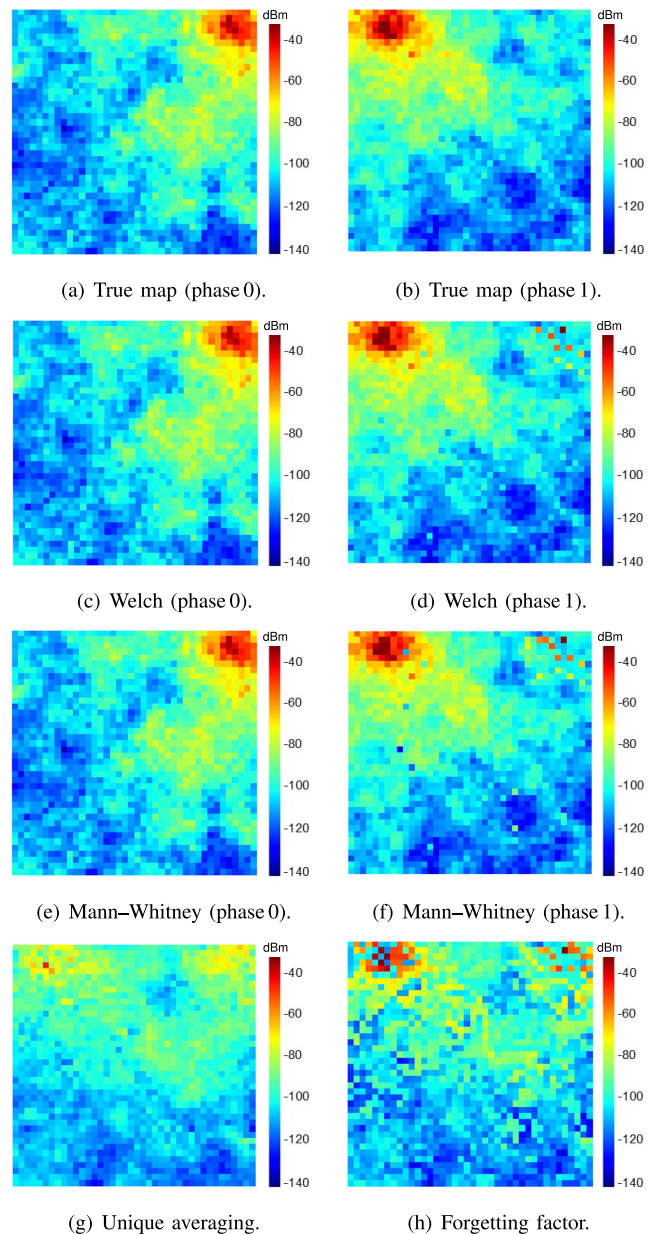(g) Unique averaging.   (h) Forgetting factor.

Fig. 4. Examples of radio maps.

it can be seen that the difference of the average received signal power between phase 0 and phase 1 is very large for several meshes in the upper left corner of the area. This is because the Mann–Whitney *U* test is inferior to Welch's *t*-test in terms of statistical power. In other words, the Mann–Whitney *U* test cannot accurately infer the significant difference between the two mean values, even if the location of the BS changes by a large distance. Thus, we argue that Welch's *t*-test should be utilized rather than a non-parametric testing method, such as the Mann–Whitney *U* test, for radio map updating.

The results of the comparison in Figs. 4(g) and 4(h) show that these two methods cannot accurately update the radio map in several meshes because these methods calculate the average
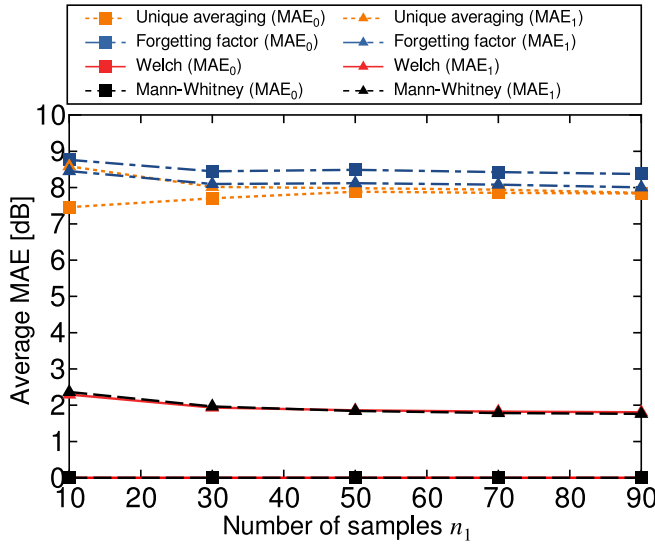
Fig. 5.   Average MAE versus the number of samples n_1.

Fig. 6.   Average MAE versus the correlation distance d_{cor}.

received signal power value without considering the movement of the BS.

B. Estimation Accuracy

Next, the estimation accuracy of the average value of the received signal power was derived for each method using the mean absolute error (MAE). In this evaluation, the MAE of each of phase 0 and phase 1 is defined as follows:

$$\mathrm{MAE}_0 = \frac{1}{D_0} \sum_{m=1}^{D_0} \left| \bar{P}_{0,\mathrm{true},m} - \bar{P}_{0,m} \right| \quad [\mathrm{dB}], \qquad (32)$$

$$\mathrm{MAE}_1 = \frac{1}{D_1} \sum_{m=1}^{D_1} \left| \bar{P}_{1,\mathrm{true},m} - \bar{P}_{1,m} \right| \quad [\mathrm{dB}], \qquad (33)$$

where $\bar{P}_{0,\mathrm{true},m}$ [dBm] and $\bar{P}_{1,\mathrm{true},m}$ [dBm] are the true average values of the received signal power of the mth mesh in phases 0 and 1, respectively. Further, $\bar{P}_{0,m}$ [dBm] and $\bar{P}_{1,m}$ [dBm] are the initial and updated average values of the received signal power of the mth mesh, respectively. In Welch's t-test and the Mann–Whitney U test, these values correspond to the average values of the received signal power in Figs. 4(c), 4(d), 4(e), and 4(f), respectively. In the comparative methods, because the initial radio map is only updated without detecting the change in the BS location, $\bar{P}_{0,m}$ and $\bar{P}_{1,m}$ correspond to the average values of the received signal power in Figs. 4(g) and 4(h), respectively. D_0 is the number of meshes in which H_0 is accepted on either Welch's t-test or the Mann–Whitney U test. D_1 is the number of meshes in which H_1 is accepted on either Welch's t-test or the Mann–Whitney U test. Considering that the main purpose of our study is to evaluate the accuracy with which the radio map can be estimated on the basis of hypothesis testing, the MAE has to be evaluated in the meshes in which each hypothesis is accepted on either Welch's t-test or the Mann–Whitney U test. Thus, D_0 and D_1 are defined separately.

It should be noted that if the root mean squared error (RMSE) is utilized, the dynamic range is significantly large
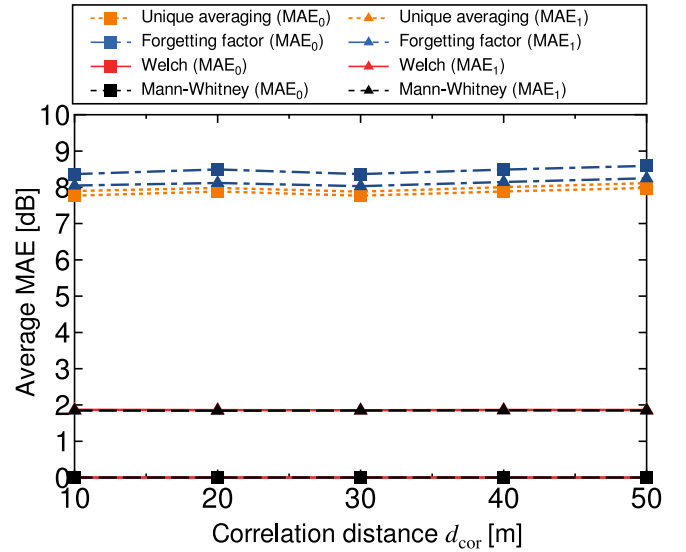
owing to the large errors in the average values of the received signal power between phases 0 and 1. Thus, the MAE was used in the evaluation. Although the RMSE uses a nonlinear approach to calculate the error, the MAE calculates the error linearly by considering the absolute error. This calculation enables the effects of the outliers to be suppressed.

Fig. 5 depicts the average MAE of each method. In this figure, the squares and triangles represent the MAE_0 and MAE_1 in each method, respectively. Here, the BS randomly moves in the simulation area for each Step (a), and d_{cor} is 20 [m]. The figure indicates that the average MAE of Welch's t-test and the Mann–Whitney U test is almost equivalent. In this simulation, because the location of the BS is randomly varied including for extremely short distances, the average MAE may not be poor in the Mann–Whitney U test. It should be noted that the MAE_0 of Welch's t-test and the Mann–Whitney U test is 0 [dB] because these methods store the initial and updated radio maps separately. Clearly, the MAEs of the methods used for the comparison are large compared with the methods based on hypothesis testing. This is because the comparative methods update the initial radio map without detecting whether the location of the BS has changed.

The average MAE versus the correlation distance d_{cor} is plotted in Fig. 6. Here, the BS was randomly moved in the simulation area for each Step (a), and n_1 is 50. These results show that the proposed method and the Mann–Whitney U test can accurately estimate the average value of the received signal power compared with the comparative methods regardless of d_{cor}. However, as shown in Section VII-A, the Mann–Whitney U test is presumed to be inferior to Welch's t-test in several meshes because of the poor statistical power.

Finally, the average MAE versus the moving distance of the transmitter is shown in Fig. 7. In this simulation, the BS was randomly moved in the simulation area using the value represented on the horizontal axis. Here, n_1 and d_{cor} are 50 and 20 [m], respectively. These results confirm that Welch's t-test and the Mann–Whitney U test can accurately estimate the
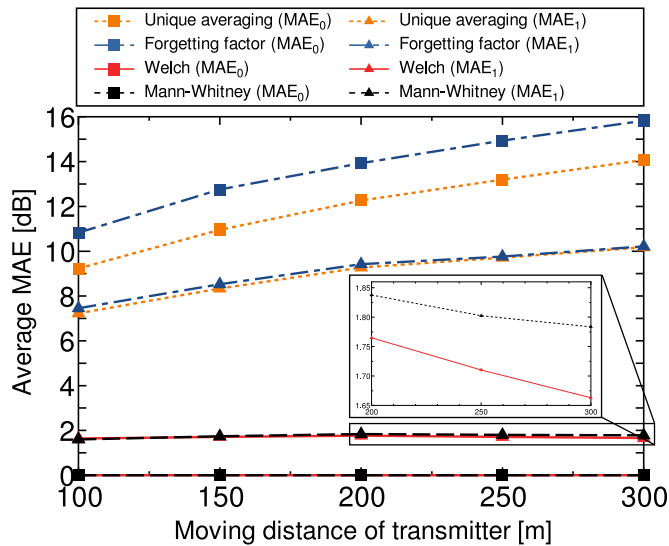
Fig. 7.   Average MAE versus moving distance of the BS.

Fig. 8.   Average MAE over a frequency-selective fading channel.

radio environment compared to the other methods. In addition, this figure indicates that the proposed method is superior to the Mann–Whitney U test. When the moving distance of the transmitter is large, the statistical power of the Mann–Whitney U test is poor compared with Welch's t-test. Thus, the average MAE is slightly degraded.

C. Effect of Radio Propagation Characteristics

The received signal power depends on factors such as the bandwidth and resource sharing methods. Thus, it is necessary to evaluate the accuracy of the proposed method by considering these factors. A strong correlation is known to exist between the average received signal power over the frequency domain [55], [56]. These results imply that *the performance of the average received signal power (and that of the proposed method) may not depend on the bandwidth and resource sharing methods.*

However, the bandwidth affects the instantaneous received signal power; therefore, we evaluated the effect of the bandwidth on the proposed method over frequency-selective fading channels. Based on the specifications of long-term evolution [57], this evaluation assumes that the transmission signal is sent over multiple resource blocks (RBs) with orthogonal frequency division multiplexing (OFDM). Each RB consists of 1.4 [MHz] bandwidth and is affected by i.i.d. Rayleigh fading.

Fig. 8 shows the average MAE versus the number of RBs. Each RB is affected by i.i.d. Rayleigh fading; therefore, the frequency selectivity is enhanced in proportion to the number of RBs. The figure shows that Welch's t-test can infer the significant difference between the two mean values with high accuracy even in the frequency-selective fading channel. This is because the deviation of the multipath fading is small compared to the difference of the path loss and the shadowing. Therefore, the proposed method may not be significantly affected by radio propagation characteristics (including path loss, shadowing, and multipath fading).
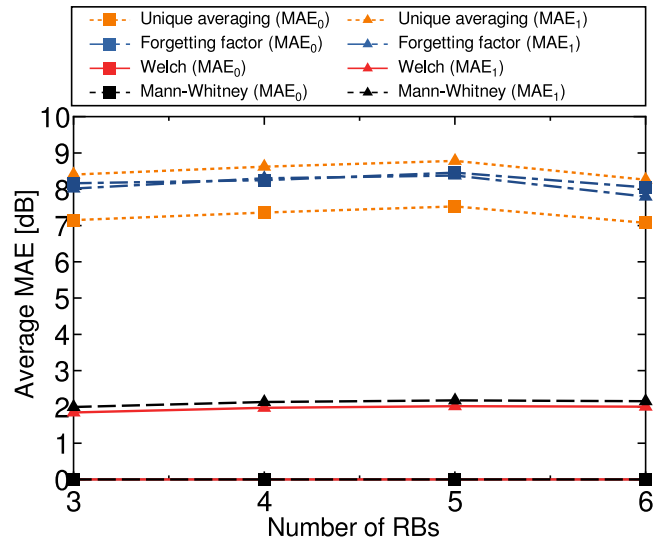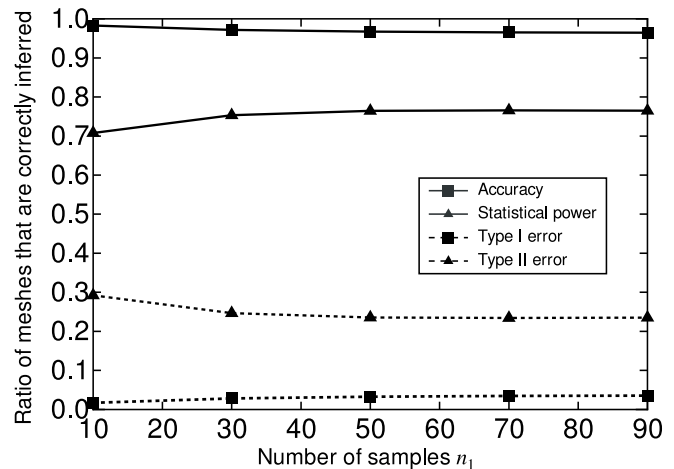

Fig. 9.   Type I and Type II errors versus n_1.

D. Type I and Type II Errors

Finally, Type I and II errors were derived using the proposed method to evaluate the accuracy of the hypothesis testing. In this evaluation, a Type I error is defined as the ratio of meshes in which the average value of the received signal power is incorrectly updated, out of all 1,600 meshes when the BS is not relocated. A Type II error is defined as the ratio of meshes in which the average value of the received signal power is not correctly updated, out of all 1,600 meshes when the BS moves. In addition, the accuracy and statistical power were derived by subtracting the Type I and II errors from 1.

The Type I and II errors are plotted in Fig. 9. Here, the BS randomly moves in the simulation area for each Step (a), and d_{cor} is 20 [m]. The figure shows that the proposed method can infer the hypothesis in most meshes when the BS does not move. However, the Type II error is larger than the Type I error because the proposed method cannot correctly update the radio map when the location of the BS only changes slightly because of the small difference in the path loss. Although the Type II error is reduced in such environments, the MAE of
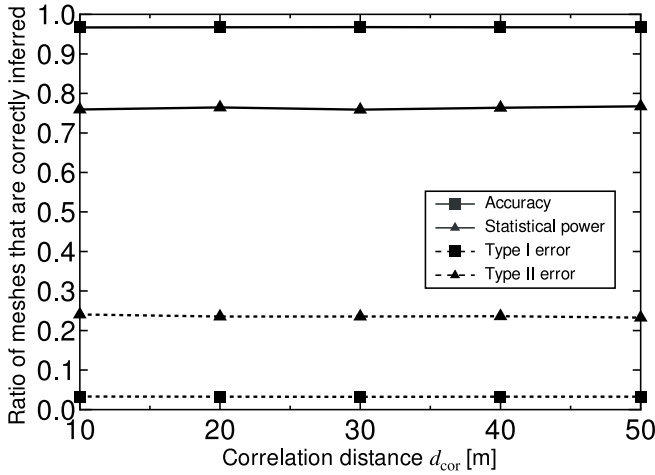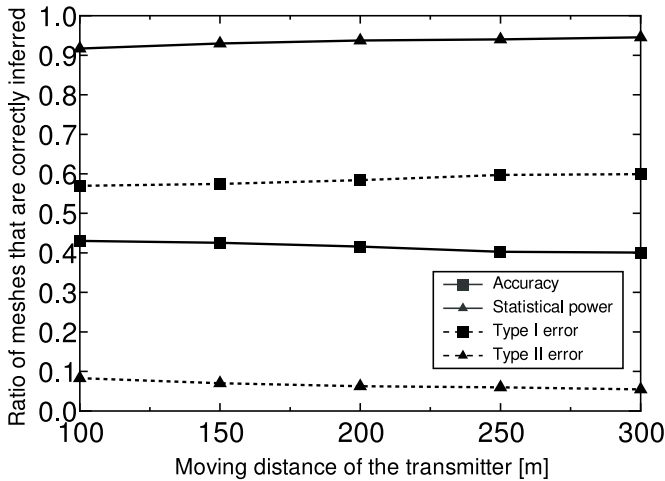
Fig. 10.   Type I and Type II errors versus d_{cor}.

Fig. 11.   Type I and Type II errors versus moving distance of the BS.

the average value of the received signal power is significantly low as shown in Fig. 7.

The Type I and II errors are additionally plotted in Fig. 10 versus d_{cor}. Here, the BS was randomly relocated in the simulation area for each Step (a), and n_1 is 50. These results show that the proposed method can accurately infer the hypothesis for approximately 80 [%] or 90 [%] of the meshes. In addition, these errors are nearly constant, regardless of the value of d_{cor}.

Finally, Fig. 11 depicts the Type I and II errors versus the moving distance of the BS. Here, n_1 and d_{cor} are 50 and 20 [m], respectively. The results in this figure confirm that the proposed method can accurately update the radio map. In addition, the Type II error can be improved as the moving distance of the BS increases because the difference in the path loss between phases 0 and 1 increases. Consequently, a significant difference in the average values of the received signal power can be confirmed, suggesting that the alternative hypothesis H_1 should be accepted.

VIII. EMULATION EVALUATION

Finally, we evaluate the performance of the proposed method using a real dataset we constructed in our early
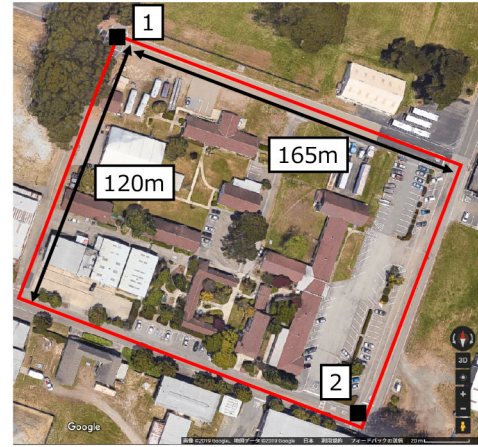

Fig. 12.   Measurement area.

TABLE II
SPECIFICATIONS OF ONBOARD UNIT

Onboard unit	MK5 OBU (Cohda Wireless)
Communication standard	IEEE 802.11p
Antenna	Omnidirectional
Center frequency [MHz]	5890
Transmission power [dBm]	24
Modulation format	BPSK, QPSK, 16QAM
Coding rate	1/2
Transmission rate [packets/s]	200
Packet length [bytes]	100, 400

work [58]. The data were acquired using outdoor vehicle-to-vehicle communication systems. Although this dataset is not applicable to cellular systems, it is suitable to demonstrate the performance of the proposed method because i) this system is able to process OFDM signals and ii) we measured the radio maps with two fixed transmitter locations (i.e., only the receiver was moved).

A. Measured Samples

This measurement was performed along California Path, UC Berkeley, USA, over two days in July 2018. In the experiments, three vehicles equipped with an onboard unit communicated with each other. The measurement route is shown in Fig. 12. The three vehicles traveled along the red line and the received signal power at each location was measured for six hours. The position of the transmitter can be obtained from the transmitted packet, and the receiver position can be extracted from the global positioning system module connected to the onboard unit. The measurement parameters are listed in Table II. The number of measured samples was 15,280,657. Details of the experiments are described elsewhere [58].

In this experiment, because all the vehicles moved dynamically along the route, an enormous number of combinations of transmission and reception positions were obtained. Had all the datasets been used for the evaluation, it would not have been possible to clarify the effectiveness of the proposed method because of the small difference in the path loss at

a short distance. Thus, two locations (points 1 and 2) were extracted for the evaluation, as shown in Fig. 12 to demonstrate the effectiveness of the proposed method. The location of the transmitter is assumed to vary from point 1 to point 2. The evaluation was performed as follows.

  A) The actual average received signal power was calculated in each 5 m mesh for each point.
  B) n_0 samples were randomly extracted in each 5 m mesh as the transmitter is positioned at point 1.
  C) Either point 1 or point 2 was randomly detected as the position of the transmitter, and the receiver was virtually deployed.
  D) The receiver observes n_1 samples from the transmitter position detected in (C).
  E) Welch's *t*-test is performed using n_0 samples and n_1 samples in each mesh. If a significant difference between the two samples is inferred, the average received signal power of the n_1 samples is calculated, and the value is registered for the reception mesh.

For evaluation, the measured samples were divided into two groups. The dataset of the first group was used to calculate the true average received signal power. Another dataset was utilized for Procedure (B) to (E). Procedures (C) to (E) were performed 1,000 times. These trials were performed 100 times, and the estimation accuracy was evaluated. The performance index of the estimation accuracy is the MAE, which is defined by

$$\text{MAE}_1 = \frac{1}{D'} \sum_{m=1}^{D'} \left| \bar{P}_{1,\text{true},m} - \bar{P}_{1,m} \right| \quad [\text{dB}], \quad (34)$$

$$\text{MAE}_2 = \frac{1}{D'} \sum_{m=1}^{D'} \left| \bar{P}_{2,\text{true},m} - \bar{P}_{2,m} \right| \quad [\text{dB}], \quad (35)$$

where $\bar{P}_{1,\text{true},m}$ [dBm] and $\bar{P}_{2,\text{true},m}$ [dBm] are the true average received signal power values of the *m*th mesh at positions 1 and 2, respectively. $\bar{P}_{1,m}$ [dBm] and $\bar{P}_{2,m}$ [dBm] are the initial and updated average values of the received signal power of the *m*th mesh, respectively. D' denotes the number of meshes used in the evaluation.

B. Emulation Results

  The evaluation results are shown in Fig. 13. These results confirm that the proposed method and the Mann–Whitney *U* test can accurately detect the change in the transmitter location in a real environment. In the measurement area shown in Fig. 12, because the communication range is narrow compared with that of the simulation parameters, the difference in the average received signal power may be small owing to the small fluctuation in the path loss. Thus, the average MAE characteristics of the proposed method are approximately equivalent to those of the Mann–Whitney *U* test. In addition, the average MAEs of the methods used for the comparison are inferior to those of the proposed method because these methods do not detect changes in the transmitter location.

  The proposed method is superior to the Mann–Whitney *U* test at $n_1 = 20$ because the statistical power of the Mann–Whitney *U* test is poor compared to that of the Welch's
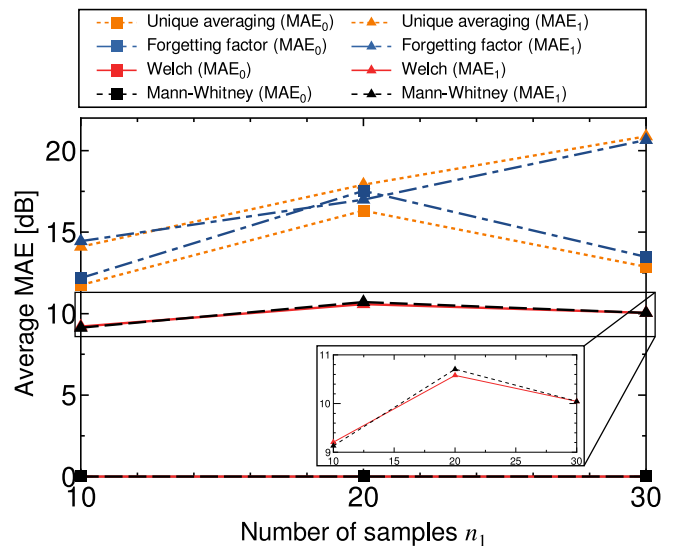

Fig. 13.   The average MAE in real environment.

t-test. However, Welch's *t*-test is slightly poor at $n_1 = 10$ because of the fluctuation in the sample mean. At the same time, we find that each MAE is equivalent to $n_1 = 30$ because increasing n_1 can improve the statistical power of the Mann–Whitney *U* test.

IX. CONCLUSION

  This study investigated radio map updating methods by taking into consideration the fact that the location of the BS is typically changed. The main technical challenge that would need to be overcome when updating the radio map in cellular systems is to devise a way in which to detect whether only real-time measurements should be used for the update. Motivated by this challenge, we proposed updating the radio map based on Welch's *t*-test, which is known to be superior to the other tests in terms of i) real-time updating, ii) no requirement to model the prior distribution, and iii) robustness for heteroscedasticity. The proposed method is designed such that the database server infers the difference in the average values of the received signal power between phases 0 and 1 using Welch's *t*-test. Both the simulation and emulation results demonstrated that the proposed method could accurately detect changes in the BS location and update the radio map.

APPENDIX

  We explain the proof of the non-central *t* distribution that was described in Section IV. To formulate the probability distribution of T_0, we first transform Eq. (16) as,

$$T_0 = \frac{\frac{\bar{X} - \bar{Y} - \delta}{\sqrt{\frac{\sigma_0^2}{n_0} + \frac{\sigma_1^2}{n_1}}} + \frac{\delta}{\sqrt{\frac{\sigma_0^2}{n_0} + \frac{\sigma_1^2}{n_1}}}}{\sqrt{\frac{d_\text{w} \frac{\frac{S_0^2}{n_0} + \frac{S_1^2}{n_1}}{\frac{\sigma_0^2}{n_0} + \frac{\sigma_1^2}{n_1}}}{d_\text{w}}}} = \frac{\frac{\bar{X} - \bar{Y} - \delta}{\sqrt{\frac{\sigma_0^2}{n_0} + \frac{\sigma_1^2}{n_1}}} + \frac{\delta}{\sqrt{\frac{\sigma_0^2}{n_0} + \frac{\sigma_1^2}{n_1}}}}{\sqrt{\frac{W}{d_\text{w}}}}, \quad (36)$$

where d_w is a constant value and corresponds to the degree of freedom of the non-central *t* distribution, which is described

later. Additionally, W is given by

$$W = d_{\mathrm{w}} \frac{\frac{S_0^2}{n_0} + \frac{S_1^2}{n_1}}{\frac{\sigma_0^2}{n_0} + \frac{\sigma_1^2}{n_1}}. \tag{37}$$

Here, $\bar{X}$ and $\bar{Y}$ follow the log-normal distribution $LN(\mu_0, \sigma_0^2/n_0)$, $LN(\mu_1, \sigma_1^2/n_1)$, respectively. By considering $\delta = \mu_0 - \mu_1$, the first term of the numerator follows the standard normal distribution in the decibel domain. Under this condition, if W follows the Chi-squared distribution with d_{w} degree of freedom, it is well known that T_0 follows the non-central t distribution and the statistical power can be formulated.

In statistics, it is difficult to formulate the probability distribution of W owing to the linear combination. Thus, the Welch–Satterthwaite equation [44] is utilized to approximate the probability distribution of W by the Chi-squared distribution. In the Welch–Satterthwaite equation, the linear combination variable Φ is given by the following equation:

$$\Phi = \sum_{i=0}^{L-1} k_i s_i^2, \tag{38}$$

where s_i^2 is a sample variable, each having v_i degree of freedom. k_i denotes the real positive number. L is the number of sample variables. In the Welch–Satterthwaite equation, the effective degree of freedom v_Φ is approximately derived as follows:

$$v_\Phi \approx \frac{\left(\sum_{i=0}^{L-1} k_i s_i^2\right)^2}{\sum_{i=0}^{L-1} \frac{\left(k_i s_i^2\right)^2}{v_i}}. \tag{39}$$

Here, in Welch's t-test, S_0^2 and S_1^2 are the unbiased sample variances, that are defined as

$$S_0^2 = \sum_{i=1}^{n_0} \frac{\left(P_{i,0} - \bar{X}\right)^2}{n_0 - 1}, \quad S_1^2 = \sum_{i=1}^{n_1} \frac{\left(P_{i,1} - \bar{Y}\right)^2}{n_1 - 1}. \tag{40}$$

The effective degree of freedom $\hat{d}_{\mathrm{w}}$ is derived by substituting $k_0 = \frac{C}{n_0}$, $k_1 = \frac{C}{n_1}$, $v_0 = n_0 - 1$, $v_1 = n_1 - 1$, $C = d_{\mathrm{w}}(\frac{\sigma_0^2}{n_0} + \frac{\sigma_1^2}{n_1})$, $s_0^2 = S_0^2$, and $s_1^2 = S_1^2$ to Eq. (39). Thus, we can get

$$\hat{d}_{\mathrm{w}} \approx \frac{\left(\frac{S_0^2}{n_0} + \frac{S_1^2}{n_1}\right)^2}{\frac{\left(\frac{S_0^2}{n_0}\right)^2}{n_0-1} + \frac{\left(\frac{S_1^2}{n_1}\right)^2}{n_1-1}}. \tag{41}$$

This approximation is based on the reference [44]. This approximation accuracy will be degraded if k_i is a negative value; however, this problem is not significant in our study because C, n_0, and n_1 are positive values. Under this approximation, we can derive that T_0 follows the non-central t distribution.

ACKNOWLEDGMENT

REFERENCES

[1] K. Katagiri and T. Fujii, "Radio environment map updating procedure based on hypothesis testing," in *Proc. IEEE DySPAN*, Newark, NJ, USA, Nov. 2019, pp. 1–6.

[2] A. Rostami, "Private 5G networks for vertical industries: Deployment and operation models," in *Proc. IEEE 2nd 5GWF*, Dresden, Germany, Sep. 2019, pp. 433–439.

[3] M. M. Blue, S. Yrjola, V. Deppanen, P. Ahokangas, H. Hammainen, and M. L. Aho, "Analysis of spectrum valuation elements for local 5G networks: Case study of 3.5-GHz band," *IEEE Trans. Cong. Commun. Netw.*, vol. 5, no. 3, pp. 741–753, Sep. 2019.

[4] C. V. Murudkar and R. D. Gitlin, "Optimal-capacity, shortest path routing in self-organizing 5G networks using machine learning," in *Proc. IEEE 20th WAMICON*, Cocoa Beach, FL, USA, Apr. 2019, pp. 1–5.

[5] S. Bi, J. Lyu, Z. Ding, and R. Zhang, "Engineering radio maps for wireless resource management," *IEEE Wireless Commun.*, vol. 26, no. 2, pp. 133–141, Apr. 2019.

[6] T. Fujii and K. Umebayashi, "Smart spectrum for future wireless world," *IEICE Trans. Commun.*, vol. E100-B, no. 9, pp. 1661–1673, Sep. 2017.

[7] Y. Zhao, J. H. Reed, S. Mao, and K. K. Bae, "Overhead analysis for radio environment map enabled cognitive radio networks," in *Proc. 1st IEEE Workshop Netw. Technol. Softw. Defined Radio Netw.*, Reston, VA, USA, Oct. 2006, pp. 18–25.

[8] X. Wang, M. Umehira, B. Han, P. Li, Y. Gu, and C. Wu, "Online incentive mechanism for crowdsourced radio environment map construction," in *Proc. IEEE ICC*, Shanghai, China, May 2019, pp. 1–6.

[9] S. H. Jung and D. Han, "Automated construction and maintenance of Wi-Fi radio maps for crowdsourcing-based indoor positioning systems," *IEEE Access*, vol. 6, pp. 1764–1777, 2017.

[10] Y. Ye and B. Wang, "RMapCS: Radio map construction from crowdsourced samples for indoor localization," *IEEE Access*, vol. 6, pp. 24224–24238, 2018.

[11] X. Ying, S. Roy, and R. Poovendran, "Pricing mechanism for quality-based radio mapping via crowdsourcing," in *Proc. IEEE GLOBECOM*, Washington, DC, USA, Dec. 2016, pp. 1–6.

[12] K. Katagiri, K. Sato, and T. Fujii, "Crowdsourcing-assisted radio environment database for V2V communications," *Sensors*, vol. 18, no. 4, p. 1183, Apr. 2018.

[13] E. Dutkiewicz, B. A. Jayawickrama, and Y. He, "Radio spectrum maps for emerging IoT and 5G networks: Applications to smart buildings," in *Proc. ICECOS*, Palembang, Indonesia, Aug. 2017, pp. 7–9.

[14] I. Kakalou, K. Psannis, S. K. Goudos, T. V. Yioultsis, N. V. Kantartzis, and Y. Ishibashi, "Radio environment maps for 5G cognitive radio network," in *Proc. MOCAST*, Thessaloniki, Greece, May 2019, pp. 1–4.

[15] E. Dutkiewicz, Y. He, B. A. Jayawickrama, and H. V. Abeywickrama, "Radio environment maps generation and spectrum sensing testbed for spectrum sharing in 5G networks," in *Proc. IEEE-APS APWC*, Verona, Italy, Sep. 2017, pp. 33–36.

[16] A. Laourine, A. Stephenne, and S. Affes, "On the capacity of log-normal fading channels," *IEEE Trans. Commun.*, vol. 57, no. 6, pp. 1603–1607, Jun. 2009.

[17] A. Ghasemi and E. S. Sousa, "Fundamental limits of spectrum-sharing in fading environments," *IEEE Trans. Wireless Commun.*, vol. 6, no. 2, pp. 649–658, Feb. 2007.

[18] K. Sato, K. Inage, and T. Fujii, "Modeling the kriging-aided spatial spectrum sharing over log-normal channels," *IEEE Wireless Commun. Lett.*, vol. 8, no. 3, pp. 749–752, Jun. 2019.

[19] A. Kliks, P. Kryszkiewicz, A. Umbert, J. P. Romero, F. Casadevall, and L. Kulacz, "Application of radio environment maps for dynamic broadband access in TV bands in urban areas," *IEEE Access*, vol. 5, pp. 19842–19863, 2017.

[20] A. Umbert, F. Casadevall, and E. G. Rodriguez, "An outdoor TV band radio environment map for a Manhattan like layout," in *Proc. ISWCS*, Poznan, Poland, Sep. 2016, pp. 399–403.

[21] Y. Huang, X. Yan, K. Chen, H. Zhou, Y. Zhang, and Z. Feng, "TV band radio environment mapping in Beijing," in *Proc. IEEE Mil. Commu. Conf.*, Baltimore, MD, USA, Oct. 2014, pp. 1675–1680.

[22] Z. Yuxian and L. Qingxia, "The construction and reconstruction of production line based on modularize," in *Proc. ICIII*, Xi'an, China, Dec. 2009, pp. 422–424.

[23] X. C. Liu, S. Zhang, H. H. Lu, and X. K. Lin, "Method for efficiently constructing and updating radio map of fingerprint positioning," in *Proc. IEEE GLOBECOM Workshops*, Miami, FL, USA, Dec. 2010, pp. 74–78.

[24] J. S. Lim, W. H. Jang, G. W. Yoon, and D. S. Han, "Radio map update automation for WiFi positioning systems," *IEEE Commun. Lett.*, vol. 17, no. 4, pp. 693–696, Mar. 2013.

[25] S. W. Ellingson, "Continuous updating of radio environment maps for millimeter-wave networks with beamforming," in *Proc. IEEE Int. Symp. Antennas Propag. USNC/URSI Nat. Radio Sci. Meeting*, San Diego, CA, USA, Jul. 2017, pp. 937–938.

[26] H. Wang, D. N. Nguyen, D. T. Hoang, E. Dutkiewics, and Q. Cheng, "Real-time crowdsourcing incentive for radio environment maps: A dynamic pricing approach," in *Proc. IEEE GLOBECOM*, Abu Dhabi, UAE, Dec. 2018, pp. 1–6.

[27] D. Zurita, E. Sala, J. A. Carino, M. Delgado, and J. A. Ortega, "Industrial process monitoring by means of recurrent neural networks and self organizing maps," in *Proc. IEEE 21st ETFA*, Berlin, Germany, Sep. 2016, pp. 1–8.

[28] S. He and S. H. G. Chan, "Wi-Fi fingerprint-based indoor positioning: Recent advances and comparisons," *IEEE Commun. Surveys Tuts.*, vol. 18, no. 1, pp. 466–490, 1st Quart., 2015.

[29] Y. Mo, Z. Zhang, W. Meng, and G. Agha, "Space division and dimensional reduction methods for indoor positioning system," in *Proc. IEEE ICC*, London, U.K., Sep. 2015, pp. 3263–3268.

[30] D. P. Turner, H. Deng, and T. T. Houle, "Statistical hypothesis testing: Overview and application," *Headache*, vol. 60, no. 2, pp. 302–308, Feb. 2020.

[31] A. Chehade and Z. Shi, "Sensor fusion via statistical hypothesis testing for prognosis and degradation analysis," *IEEE Trans. Autom. Sci. Eng.*, vol. 16, no. 4, pp. 1774–1787, Feb. 2019.

[32] M. Korki, H. Zayyani, and J. Zhang, "Bayesian hypothesis testing for block sparse signal recovery," *IEEE Commun. Lett.*, vol. 20, no. 3, pp. 494–497, Mar. 2016.

[33] H. Zayyani, M. B. Zadeh, and C. Jutten, "Bayesian pursuit algorithm for sparse representation," in *Proc. IEEE ICASSP*, Taipei, Taiwan, Apr. 2009, pp. 1549–1552.

[34] T. Halme, M. Golz, and V. Koivunen, "Bayesian multiple hypothesis testing for distributed detection in sensor networks," in *Proc. IEEE Data Sci. Workshop*, Minneapolis, MN, USA, Jun. 2019, pp. 105–109.

[35] J. Wahlstrom, I. Skog, F. Gustafsson, A. Markham, and N. Trigoni, "Zero-velocity detection-A Bayesian approach to adaptive thresholding," *IEEE Sens. Lett.*, vol. 3, no. 6, pp. 1–4, Jun. 2019.

[36] T. Lumley, P. Diehr, S. Emerson, and L. Chen, "The importance of the normality assumption large public health data sets," *Annu. Rev. Public Health*, vol. 23, pp. 151–171, Feb. 2002.

[37] U. Palukha and Y. Kharin, "Performance analysis for statistical testing of random and pseudorandom generators by entropy statistics," in *Proc. IDT*, Zilina, Slovakia, Jun. 2019, pp. 358–364.

[38] H. P. Nguyen, A. Delahaies, F. Retraint, D. H. Nguyen, M. Pic, and F. M. Nicolier, "A watermarking technique to secure printed QR codes using a statistical test," in *Proc. IEEE GlobalSIP*, Nov. 2017, pp. 288–292.

[39] M. R. Leonard, M. Stiefel, M. FunB, and A. M. Xoubir, "Robust sequential testing of multiple hypotheses in distributed sensor networks," in *Proc. IEEE ICASSP*, Calgary, AB, Canada, Apr. 2018, pp. 4394–4398.

[40] D. W. Zimmerman, "Inflation of Type I error rates by unequal variances associated with parametric, nonparametric, and rank-transformation tests," *Psicologica*, vol. 25, no. 1, pp. 103–133, Jan. 2004.

[41] V. Immler, M. Hiller, J. Obermaier, and G. Sigl, "Take a moment and have some T: Hypothesis testing on raw PUF data," in *Proc. IEEE HOST*, McLean, VA, USA, May, 2017, pp. 128–129.

[42] Z. Fang, Z. Zhao, D. Geng, Y. Xuan, L. Du, and X. Cui, "RSSI variability characterization and calibration method in wireless sensor network," in *Proc. ICINFA*, Harbin, Jun. 2010, pp. 1532–1537.

[43] G. D. Ruxton, "The unequal variance t-test is an underused alternative to Student's t-test and the Mann–Whitney U test," *Behav. Ecol.*, vol. 17, no. 4, pp. 688–690, May 2006.

[44] F. E. Satterthwaite, "An approximate distribution of estimates of variance components," *Biometr. Bull.*, vol. 2, no. 6, pp. 110–114, Dec. 1946.

[45] A. Achtzehn, J. Riihijärvi, and P. Mähönen, "Improving accuracy for TVWS geolocation databases: Results from measurement-driven estimation approaches," in *Proc. IEEE DySPAN*, McLean, VA, USA, Apr. 2014, pp. 392–403.

[46] M. Barrie, S. Delaere, G. Sukarevicienè, J. Gesquiere, and I. Moerman, "Geolocation database beyond TV white spaces? Matching applications with database requirements," in *Proc. IEEE DySPAN*, Bellevue, WA, USA, Oct. 2012, pp. 467–478.

[47] J. Dai, A. Xu, X. Liu, C. Yu, and Y. Wu, "Online sequential model for multivariate time series prediction with adaptive forgetting factor," *IEEE Access*, vol. 8, pp. 175958–175971, Sep. 2020.

[48] W. Cao, Z. Ming, Z. Xu, J. Zhang, and Q. Wang, "Online sequential extreme learning machine with dynamic forgetting factor," *IEEE Access*, vol. 7, pp. 179746–179757, Dec. 2019.

[49] C. Yang and H. Fang, "A new nonlinear model-based fault detection method using Mann–Whitney test," *IEEE Trans. Ind. Electron.*, vol. 67, no. 12, pp. 10856–10864, Dec. 2019.

[50] Y. Wang and L. Tian, "The equivalence between Mann–Whitney Wilcoxon test and score test based on the proportional odds model for ordinal responses," in *Proc. 4th IEIS*, Kyoto, Japan, Jul. 2017, pp. 1–5.

[51] M. Zhou, Y. Wang, Z. Tian, and Q. Zhang, "Marvel: Mann–Whitney rank-sum testing via segments labeling for indoor pedestrian localization," in *Proc. IEEE ICC*, Kansas City, MO, USA, May 2018, pp. 1–6.

[52] D. Rasch, K. D. Kubinger, and K. Moder, "The two-sample *t* test: Pretesting its assumptions does not pay off," *Stat. Paper*, vol. 52, no. 1, pp. 219–231, Feb. 2011.

[53] M. Gudmundson, "Correlation model for shadow fading in mobile radio systems," *Electron Lett.*, vol. 27, no. 23, pp. 2145–2146, Nov. 1991.

[54] R. Zhang, J. Wei, D. G. Michelson, and V. C. M. Leung, "Outage probability of MRC diversity over correlated shadowed fading channels," *IEEE Wireless Commun. Lett.*, vol. 1, no. 5, pp. 516–519, Jul. 2012.

[55] P. E. Mogensen, P. Eggers, C. Jensen, and J. B. Andersen, "Urban area radio propagation measurements at 955 and 1845 MHz for small and micro cells," in *Proc. IEEE GLOBECOM*, Phoenix, AZ, USA, Dec. 1991, pp. 1297–1302.

[56] B. Van Laethem, F. Quitin, F. Bellens, C. Oestges, and P. De Doncker, "Correlation for multi-frequency propagation in urban environments," *Progr. Electromagn. Res. Lett.*, vol. 29, no. 2, pp. 151–156, Jan. 2012.

[57] K. P. Snehal and M. G. Shajan, "Efficient resource allocation in downlink LTE networks," in *Proc. 5th Int. Conf. Commun. Syst. Netw. Technol.*, Gwalior, India, Apr. 2015, pp. 190–193.

[58] K. Katagiri and T. Fujii, "Demo: Highly accurate prediction of radio environment for V2V communications," in *Proc. IEEE DySPAN*, Newark, NJ, USA, Nov. 2019, pp. 1–2.

Keita Katagiri (Student Member, IEEE) was born in Kagawa, Japan, in 1994. He received the B.E. and M.E. degrees in electrical engineering from the University of Electro-Communications in 2017 and 2019, respectively, where he is currently pursuing the Ph.D. degree. Since 2019, he has been a Research Fellow (DC1) with the Japan Society for the Promotion of Science. His current research interest includes radio map. He received the Best Demo Award for IEEE DySPAN 2019.

Koya Sato (Member, IEEE) was born in Miyagi, Japan, in 1991. He received the B.E. degree in electrical engineering from Yamagata University in 2013, and the M.E. and Ph.D. degrees from the University of Electro-Communications in 2015 and 2018, respectively. From 2017 to 2018, he was a Research Fellow (DC2) with the Japan Society for the Promotion of Science. He is currently an Assistant Professor with the Tokyo University of Science. His current research interests include wireless communications, decentralized machine learning, data privacy, and spatial statistics.

Kei Inage (Member, IEEE) was born in Chiba, Japan, in 1986. He received the B.E. and M.E. degrees in electronic engineering and the Ph.D. degree in communication engineering and informatics from the University of Electro-Communications, Japan, in 2009, 2011, and 2014, respectively. From 2012 to 2014, he was a Research Fellow (DC2) with the Japan Society for the Promotion of Science. From 2014 to 2015, he was a Researcher with the Smart Wireless Laboratory, Wireless Network Research Institute, and National Institute of Information and Communications Technology. From 2015 to 2018, he was an Assistant Professor with the Electrical and Electronics Engineering Program, Tokyo Metropolitan College of Industrial Technology, where he is currently an Associate Professor. His current research interests include spectrum sharing and ad hoc networks. He received the Young Researcher's Award from IEICE in 2012.

Takeo Fujii (Member, IEEE) was born in Tokyo, Japan, in 1974. He received the B.E., M.E., and Ph.D. degrees in electrical engineering from Keio University, Yokohama, Japan, in 1997, 1999, and 2002, respectively, where he was a Research Associate with the Department of Information and Computer Science from 2000 to 2002. From 2002 to 2006, he was an Assistant Professor with the Department of Electrical and Electronic Engineering, Tokyo University of Agriculture and Technology. From 2006 to 2014, he was an Associate Professor with the Advanced Wireless Communication Research Center, University of Electro-Communications, where he is currently a Professor. His current research interests include cognitive radio and ad hoc wireless networks. He was a recipient of the Best Paper Award for the IEEE VTC 1999-Fall, the 2001 Active Research Award in Radio Communication Systems from the IEICE Technical Committee of RCS, the 2001 Ericsson Young Scientist Award, the Young Researcher's Award from IEICE in 2004, the Young Researcher Study Encouragement Award from the IEICE Technical Committee of AN in 2009, the Best Paper Award for IEEE CCNC 2013, and the IEICE Communication Society Best Paper Award in 2016.